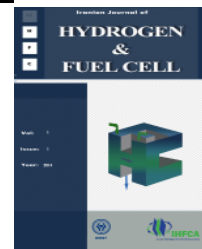


Iranian Journal of Hydrogen & Fuel Cell

IJHFC

Journal homepage://ijhfc.irost.ir



## Theoretical study of the effect of hydrogen addition to natural gas-fueled direct-injection engines

Javad Zareei<sup>1,\*</sup>, Faizal Wan Mahmood<sup>1</sup>, Shahrir Abdullah<sup>1</sup>, Hj. Yusoff Ali<sup>1</sup>

<sup>1</sup>Center for Automotive Research, Faculty of Engineering and the Built Environment, University Kebangsaan Malaysia

### Article Information

Article History:

Received:

19 July 2013

Received in revised form:

22 November 2013

Accepted

13 January 2014

### Keywords

compressed natural gas

hydrogen

spark ignition engine

direct injection

### Abstract

The preparation of air–fuel mixture to achieve improved performance, efficiency, and engine combustion is considerably dependent on fluid flow dynamics. In this study, the effects of mixtures of hydrogen and compressed natural gas (CNG) on a spark ignition engine are numerically considered. This article presents the results of a direct-injection engine using methane–hydrogen mixtures containing 0 and 15 vol.% H<sub>2</sub>. The results show that the percentage of hydrogen in the CNG increases the burning velocity of CNG and reduces the optimal ignition timing to obtain the maximum peak pressure of an engine running with a blend of hydrogen and CNG.

With hydrogen addition to natural gas, the peak heat release rates increase. For 15% hydrogen, the maximum values at crank angles (CAs) for in-cylinder temperature and heat release rate are achieved at 8° CA, and the maximum temperature difference is approximately 150 K. Port injection gasoline is converted into direct injection by CNG fuel in this engine.

## 1. Introduction

Growing concerns on the harmful effects of conventional fossil fuel emissions have made natural gas (NG) a very attractive alternative fuel for internal combustion engines (ICEs), particularly for its advantages, which include being environment friendly, clean burning, economical, and efficient. For light-duty engine applications in particular, the direct injection (DI) of compressed NG (CNG) achieves thermal efficiencies comparable with those accomplished by high-compression-ratio, unthrottled diesel engines, while maintaining the smoke-free operation of spark ignition (SI) engines and producing slightly lower NO<sub>x</sub> emissions [1]. NG is one of the most promising of alternative fuels, providing lower cost, cleaner emissions, and direct applicability to existing combustion systems. However, the use of natural gas as fuel in

tion (DI) of compressed NG (CNG) achieves thermal efficiencies comparable with those accomplished by high-compression-ratio, unthrottled diesel engines, while maintaining the smoke-free operation of spark ignition (SI) engines and producing slightly lower NO<sub>x</sub> emissions [1]. NG is one of the most promising of alternative fuels, providing lower cost, cleaner emissions, and direct applicability to existing combustion systems. However, the use of natural gas as fuel in

\*Corresponding author. E-mail: ja\_zareei@iust.ac.ir  
Tel: +989127235978

ICEs can adversely affect engine performance [2].

The power of these engines are relatively less than that of engines that are primarily fueled by gasoline because of the convergence of one or several factors: a reduction in volumetric efficiency attributed to NG injection in the intake manifold; lower stoichiometric fuel/air ratio of NG compared with gasoline; and lower equivalence ratio at which these engines may be run to reduce NO<sub>x</sub> emissions. High NO<sub>x</sub> emissions, particularly at high loads, decrease with exhaust gas recirculation (EGR). However, EGR rates above a maximum value result in misfire and erratic engine operation.

The addition of hydrogen gas increases this EGR threshold significantly. In addition, hydrogen increases the flame speed of the NG–hydrogen mixture.

Hydrogen gas is characterized by a rapid combustion speed, wide combustible limit, and low minimum ignition energy. Such characteristics serve a function in decreasing engine cycle variation for the safety of combustion. However, the values of cycle variation for hydrogen-fueled engines with DI are frequently higher than those of hydrogen-fueled engines with manifold injection, or those of gasoline engines because of a decrease in the mixing period by DI in the process of hydrogen gas compression [3–5].

The percentage of hydrogen in H<sub>2</sub>CNG mixture increases the burning velocity of NG and decreases the optimal ignition timing to obtain the maximum indicated mean pressure of the engine running with these mixtures. The indicated efficiency rises as the percentage of hydrogen in NG increases [6]. Increasing the hydrogen fraction causes variations in cylinder pressure and CO<sub>2</sub> emissions. Emilio Navarro et al. [7] showed that the maximum cylinder pressure increases with the fraction of hydrogen in the blend. The presence of hydrogen in the blend decreases CO<sub>2</sub> emissions. Owing to the properties of hydrogen, leaner fuel–air mixtures can be used along with the appropriate spark timing, resulting in an improvement in engine emissions with no loss of performance.

Yilanci et al. and Weindorf et al. [8, 9] studied the alternative use of hydrogen in various governmental strategic plans as an energy carrier to achieve a sustainable energy system. Hydrogen is a good option because of the various methods of its production, the long-term feasibility of a number of these methods (from nuclear power, from renewable energy: solar, wind, biomass,

fossil fuels, and so on), high potential efficiency at its use point, various energy production methods from hydrogen, and almost no dangerous emissions [10]. Nitrogen oxides formation and flame propagation were calculated for two engines with hydrogen fuel through an internal computational fluid dynamics (CFD) code, with a correlation of laminar burning velocity and a model of flame area evolution [11]. The use of laminar burning velocities obtained through calculations of chemical kinetic was also investigated. Except for increased engine velocity and conditions of lean mixture, fair consensus was found among experimental findings. According to the researchers, the results “suggest the requirement for the consideration of an increase in local laminar burning velocity due to the selective diffusion of hydrogen.”

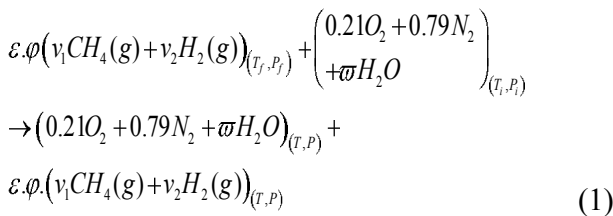
The results of a four-cylinder engine test with mixtures of 0, 10, 20, and 30 vol.% hydrogen in methane showed that HC, CO, and CO<sub>2</sub> emission values decreased, but NO and brake thermal efficiency values increased with increasing percentage of hydrogen [12]. The enhancement of combustion with hydrogen addition can be ascribed to the significant increase in H, O, and OH in the flame with the presence of hydrogen. The decrease in the mole fractions of CH<sub>2</sub>O and CH<sub>3</sub>CHO with hydrogen addition suggests a potential in the reduction of aldehyde emissions of methane combustion as hydrogen is added [13]. Hoekstra et al. [14] observed that experimental results of NG-fueled ICEs suggest that hydrogen as an additive in NG can strongly improve the performance of such engines, particularly in terms of power, efficiency, and emissions, thus enabling the engine to work with leaner mixtures. In addition, hydrogen does not affect the anti-knocking performance of NG fuel and induces a strong reduction of NO<sub>x</sub> for hydrogen percentages of up to 30%. An important point is the increasing flame speed propagation and a consequent reduction in the spark advance angle to obtain the maximum brake torque, as already indicated by Nagalingam et al. [15].

Hydrogen–NG blends, commonly called HCNG, can be distributed using NG infrastructures without significant modifications if hydrogen content is below 30 vol.%. Mariani et al. [16] showed that HCNG blends improved engine brake efficiency, particularly at low loads and for the highest hydrogen content, with fuel consumptions on an energy basis over NEDC being 2.5, 4.7, and 5.7% lower than that of CNG for HCNG that are 10, 20, and 30%, respectively.

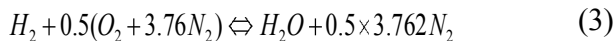
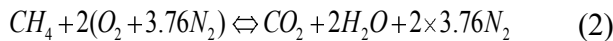
## 2. Thermophysical properties:

The thermo physical properties of fluid(s), including thermal conductivity, viscosity, density, specific heat, and species diffusivities, as functions of concentration and temperature as well as other variables are provided by the STAR-CD modeling framework. Alternative built-in dependencies are provided in some cases, but facilities are generally available to insert user-specified property functions.

Fuel is combined with air after being introduced into the intake manifold. The process follows the subsequent chemical equation:



The chemical equations for the combustion of stoichiometric hydrogen–air and methane–air mixtures are as follows:



In the above equations,  $\phi$  represents the total number of fuel moles,  $\phi$  is the ratio of fuel/air equivalence,  $v_i$  corresponds to component  $i$  mole quantity per fuel mixture mole, and  $\varpi$  stands for ratio of molar humidity. When pure hydrogen is used,  $v_i=0$ ; but, if pure NG is used,  $v_2=0$ .

The first law of thermodynamics is applied to the process of mixing to calculate the thermodynamic properties of the air–fuel mixture. Potential energies and kinetic variations are ignored, and it is assumed that no work is performed throughout the process. The equation would be:

$$\begin{aligned} & \sum_{n=1}^N \varepsilon.\phi.v_1 \left[ \int_{T_0}^T C_{P_i}^0(T) dT - \int_{T_0}^{T_f} C_{P_i}^0(T) dT \right] + \\ & 0.21 \left[ \int_{T_0}^T C_{P_{O_2}}^0(T) dT - \int_{T_0}^{T_i} C_{P_{O_2}}^0(T) dT \right] \\ & + 0.79 \left[ \int_{T_0}^T C_{P_{N_2}}^0(T) dT - \int_{T_0}^{T_i} C_{P_{N_2}}^0(T) dT \right] + \\ & \varpi \left[ \int_{T_0}^T C_{P_{H_2O}}^0(T) dT - \int_{T_0}^{T_i} C_{P_{H_2O}}^0(T) dT \right] - Q = 0 \end{aligned} \quad (4)$$

where  $Q$  represents heat transfer during the process,  $C_{pi}^0$  is the constant-pressure specific ther-

mal capacity of an ideal gas [17],  $T_f$  stands for the fuel temperature before injection,  $T_0$  is reference temperature (298.15 K), and corresponds to the temperature of intake air.

The calculated air–fuel mixture is then introduced into the cylinder. The residual gas mixing process inside the cylinder and the entrance of the air–fuel mixture in the cylinder occur during this phase.

## 3. Combustion modelling

Diffusion or un-premixed reaction was employed to replicate the CNG combustion process. The employed mono-fuel (methane) was catalyzed the diffusion reaction usage for this engine model. The oxidant streams and fuel entered the engine cylinder separately in this reaction as the solution domain. For every reaction, one more differential conservation equation must be solved. The mixture fraction ( $f$ ), that is, the preferred conserved scalar, is basically described as the total mass fraction of unburnt and burnt fuels. The following equation in the tensor notation can be used to calculate  $F$ :

$$\frac{\partial}{\partial t}(\rho f) + \frac{\partial}{\partial x_j} \left[ \rho \mu_{j,f} - \left( \rho D_f + \frac{\mu_t}{\sigma_{f,t}} \right) \frac{\partial f}{\partial x_j} \right] = S \quad (5)$$

In this equation, the turbulent Schmidt number is  $\sigma_{f,t}$ ; and the source term  $S$  corresponds to the fuel addition to the gaseous phase origin from a second phase, such as coal particles or diesel fuel droplets.

In this study, the eddy break-up (EBU) model of Magnussen was employed to simulate the combustion of turbulence [18]. The EBU model could be used for all combustion applications. The two main assumptions of this model are as follows: (1) a reaction is an irreversible single-step reaction involving products, oxidant, and fuel in addition to potential background static species; and (2). as the rate-controlling mechanism is turbulent micro mixing, time scale of the reaction is very small. The rate of fuel consumption based on the employed model was as follows:

$$R_F = -\frac{\rho \mathcal{E}}{k} A_{ebu} \min \left[ Y_F, \frac{Y_O}{s_O}, B_{ebu} \frac{Y_P}{s_P} \right] \text{kg/m}^3\text{s} \quad (6)$$

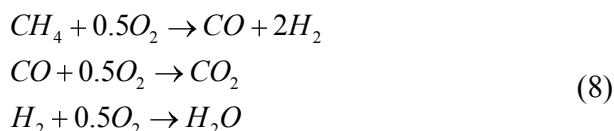
$$s_O \equiv \frac{n_O M_O}{n_F M_F}, s_P \equiv \frac{n_P M_P}{n_F M_F} \quad (7)$$

where the empirical coefficients of dimensions are  $B_{ebu}$  and  $A_{ebu}$ . According to the burned mass

fraction of fuel during combustion, the nominal default values are 0.8 and 1.2, respectively. The local rate-controlling mass fraction is determined by the first two arguments in the square brackets. However, the third argument inhibits the reaction in case of low temperature. This argument could be optionally deleted. The micro mixing time scale was assumed to be  $k/\varepsilon$ , as the time scale of dissipation.

### 3.1. Mechanism of reaction

The three-step global reaction of the EBU model was the basis for the modeling strategy for combustion modelled by the CFD model. The equations for the three steps are as follows:



The properties of individual species are used to calculate the specific heat of mixture, thermal conductivity, and viscosity, all of which are functions of temperature. The mass fractions of the combustion products are assumed to obey the values of instantaneous and local thermodynamic equilibrium. The ratio of temperature, pressure, and equivalence determine equilibrium composition of cylinder charge [19].  $O_2$ ,  $CO_2$ ,  $H_2O$ ,  $N_2$ ,  $H_2$ ,  $CO$ , and  $NO$  were the considered chemical species for the calculation of CFD, and NG was deemed as 100% methane ( $CH_4$ ).

## 4. Geometry of engine and its operating condition

According to Figure 1, the engine model used in this study was a typical CNGDI engine with a single cylinder and two exhaust and intake valves. As shown in Figure 2, it has two pistons of different shapes. Two different piston crowns were considered to examine the pattern and behavior of turbulence, tumble, and swirl intensity field inside the cylinder to attain a suitable piston shape for the engine combustion process. The piston shapes indicated the geometry model of a real engine which is usually operated to achieve a higher ratio of compression and the optimum process of combustion in a CNGDI engine. Two different piston shapes were examined to verify a suitable piston crown for the analysis of heat transfer and turbulence char-

acteristics, and for preparation of fuel mixing for the subsequent best combustion process. A bowl was positioned at the center of piston A crown. The bowl volume of piston B was deeper, but it was not positioned in the crown center.



Figure 1. Schematic view of typical engine model with piston crown A

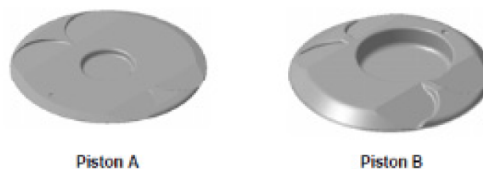


Figure 2. Geometry of the combustion chambers on pistons

## 5. Grid generation

In this study, the moving mesh-boundary algorithm was used to perform CFD simulations of the combustion process. Each event in the boundary and moving mesh algorithms corresponded to different boundary and mesh geometries for each different crank angle (CA) in every engine cycle step [20]. Therefore, appropriate CFD simulations for an internal process of combustion required that the calculation and analysis be performed through the moving meshes and boundaries, transient (unsteady) calculation, high fluid dynamic characteristics (turbulence intensity), high compressible Reynolds number, heat, mass, momentum, transfer, as well as through a chemical-thermal dependent and complex geometry model. The process of grid generation was initiated from the mesh surface provision of the engine developed in a computer-aided design (CAD) program. Thereafter, to deal with the CFD analysis, the surface data should be converted into a finite volume mesh. A grid generator program was used to generate hexahedral cells for the CFD calculation of computational mesh in this study. As shown in Figure 3a, the mesh involves the valves

and intake ports, piston bowl, and cylinder head. The parallel computations are shown by different colors, representing four computation processes. The cell numbers varied between 90,000 in the top dead center (TDC) and approximately 180,000 to 200,000 in the bottom dead center (BDC). Approximately half of the cells were employed to create the mesh at the piston bowl and cylinder head when the rational computer run time and grid sensitivity were considered. During the valve movement, fine grid arrangement was required to meet the convergence and stability criteria. Owing to their better stability and accuracy compared with tetrahedral cells, hexahedral cells were applied for mesh generation. A more important reason for the use of hexahedral cells was that moving meshes and boundaries are required to accomplish CFD calculation.

Owing to the model complexity, four areas with different topologies were assumed for the computational domain and, as shown in the wire mesh view, every area was meshed individually (Figure 3). This approach helped reduce the meshing time considerably to acquire a quality grid (mesh). Arbitrary interfaces were employed to ensure the connectivity of different sub-domains, which connected each face of the zones. Similar topology was used to create meshes of both intake ports, and the cell was oriented in the direction of flow and connected with a cylindrical structured mesh in the valve zone upstream. The grid above the valves (both exhaust and intake) was created through the revolution of a structure mesh section. The sub-domains of intake ports were removed from the calculation during the compression stroke with closed intake valves to decrease computational cost and time.

To achieve a reasonable computer run time and grid sensitivity, the fine grid structure was required for mesh snap ping during the valve movement.

Hexahedral cells offer better stability and accuracy compared to tetrahedral cells. Thus, hexahedral cells were employed for mesh generation. Hexahedral cells were principally used because of the requirements of boundaries and moving meshes for CFD calculation. The computational mesh was split into four areas with different topologies because of complexity of the engine model, and every area was meshed individually, resulting in good grid (mesh) quality and a significant reduction in meshing time. Arbitrary interfaces were used to ensure the connectivity of various sub-domains that united each Arbitrary interfaces were used to ensure the connectivity

ping during the valve movement.

Hexahedral cells offer better stability and accuracy compared to tetrahedral cells. Thus, hexahedral cells were employed for mesh generation. Hexahedral cells were principally used because of the requirements of boundaries and moving meshes for CFD calculation. The computational mesh was split into four areas with different topologies because of complexity of the engine model, and every area was meshed individually, resulting in good grid (mesh) quality and a significant reduction in meshing time. Arbitrary interfaces were used to ensure the connectivity of various sub-domains that united each Arbitrary interfaces were used to ensure the connectivity of various sub-domains that united each face of the zones.

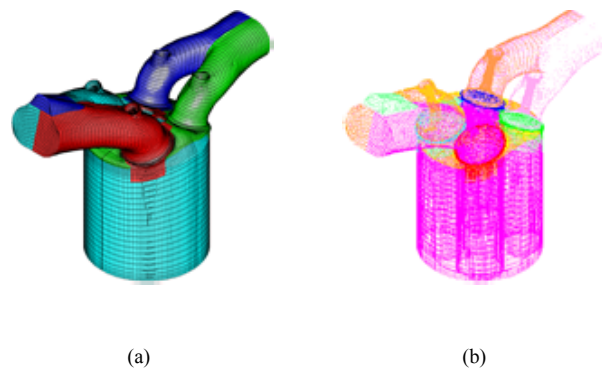


Figure 3. Schematic view and wire

*mesh of the computational grid at BDC*

As previously stated, embedding a boundary and moving mesh algorithm into the Star-CD program was necessary for simulation. The boundary and moving mesh algorithm for such an engine model was developed inside Star-CD through the declaration of events for every defined time step followed by activation of the grid to facilitate mesh movement. In the moving mesh, the cell was compressed to volume zero in one time step, and all the contents (temperature, enthalpy, pressure, momentum, mass, and so on) were forced into the adjacent cells. Thus, even if any of cell layers was removed, conservation would be precisely satisfied. However, according to Adapco [21], the size of cell layers increases from zero to the full volume when they are added through absorption of the preserved variables through cell faces. Figure 4 demonstrates some examples of the developed boundaries and moving meshes for the CFD simulation model, including compression stroke, piston position at BDC, and intake stroke.

The overall quantity of computational cells is

approximately 180,000 to 200,000. This, approximately requires 8 hours for a typical CPU to simulate complete compression stroke and intake by fluctuating time steps using a six CPU-SGI Origin 300 with dynamic memory of 56 MB.

## 6. Experiments

A single-cylinder engine based on the Proton CAMPRO engine was modified into a CNG-fueled engine with DI system. The engine was operated under wide-open throttle conditions with a compression ratio of 14:1. The main specifications of the engine are given in Table 1.

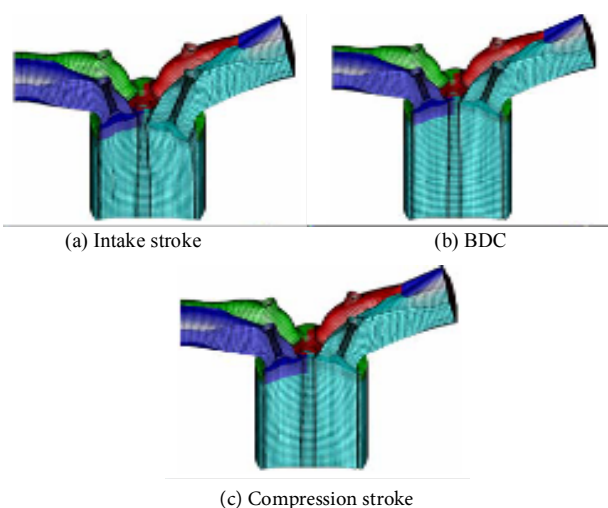


Figure 4. Moving mesh and boundary

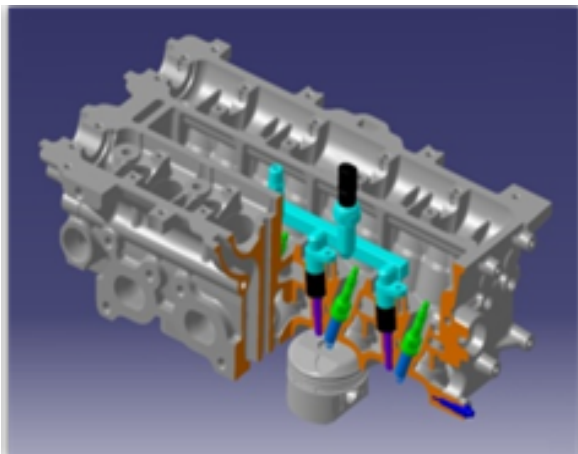


Figure 5. 3D CAD modeling of CNGDI components

The experimental cases chosen for the validation of the CFD model included both low and high engine speeds, that is, 2000 and 6000 rpm, respectively, with certain variations in intake temperature, injection timing, injection duration, and SI timing.

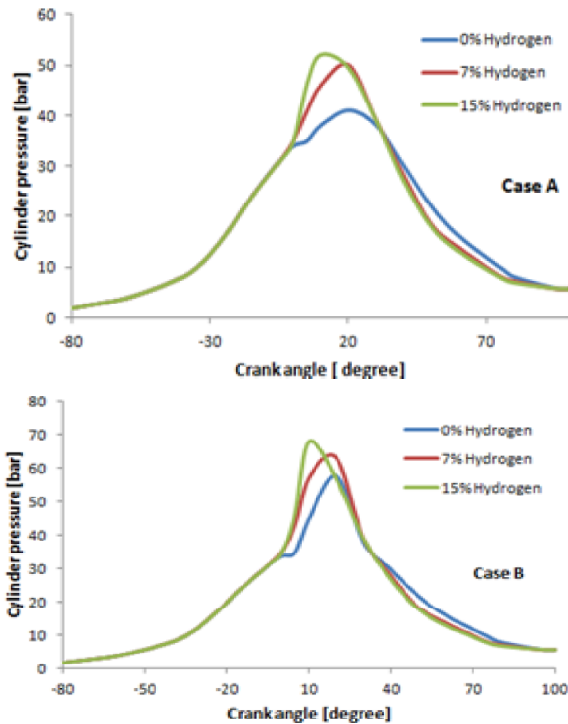
## 7. Results and discussions

Figure 6 presents the cylinder pressure versus the CA. The peak cylinder pressure increased and appeared with the advancement of CAs and with the addition of increasing amounts of hydrogen. In particular, for 15% hydrogen, the peak cylinder pressure increased by approximately 11 bar compared with that for 0% hydrogen at 2000 rpm. The peak appeared at an advanced CA, that is, approximately  $10^{\circ}\text{CA}$  close to the TDC and  $10^{\circ}\text{CA}$  after the TDC. As shown in Figure 7, when hydrogen addition to methane is increased, the maximum peak pressure values are found to be close to the TDC.

Table 1. Geometric properties of CNG/DI engine

| Engine parameter           | Unit   | Value           |
|----------------------------|--------|-----------------|
| Number of cylinders        | 4      | -               |
| Type                       | Inline | -               |
| Displacement volume        | 1596   | cm <sup>3</sup> |
| Bore                       | 78     | mm              |
| Stroke                     | 84     | mm              |
| Connecting rod length      | 131    | mm              |
| Crank radius               | 44     | mm              |
| Compression ratio          | 14:1   | -               |
| Intake valve opening       | 12     | bTDC            |
| Intake valve closing       | 48     | aBDC            |
| Exhaust valve opening      | 45     | bBDC            |
| Exhaust valve closing      | 10     | aTDC            |
| Maximum exhaust valve lift | 7.5    | mm              |

The maximum peak pressure values are obtained at an engine speed of 6000 rpm.



**Figure 6.** Cylinder pressure as function of the CA at a fixed EAR of unit with different percentage of hydrogen and spark timing of 19CA BTDC at 2000 (case A) and 6000 rpm (case B)

The in-cylinder temperature (Figure 7) increased because of the high adiabatic flame temperature. For 15% hydrogen, the maximum values for in-cylinder temperature and heat release rate were advanced by approximately 8° CA compared with the corresponding CA for 0% hydrogen. The maximum temperature difference between the 0% H<sub>2</sub> and 15% H<sub>2</sub> cases was approximately 150 K because the laminar flame speed of a methane and hydrogen blend increases with hydrogen addition for a fixed excess air ratio.

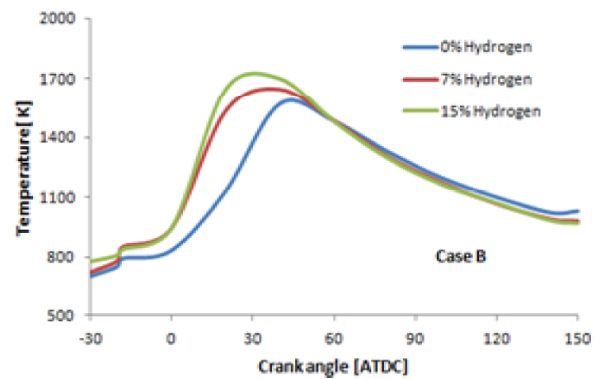
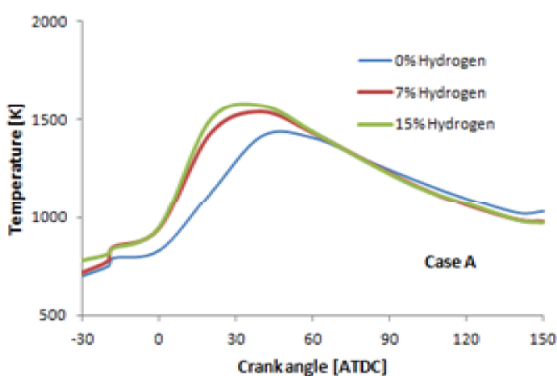


**Figure 7.** Cylinder temperature versus the CA at a fixed EAR of unit and spark timing of 19°CA BTDC at 2000 (case A) and 6000 rpm(case B)

The heat release rate is defined as the rate at which the chemical energy of the fuel is released by the combustion process. This rate is calculated from the cylinder pressure versus CA as the energy release required creating the measured pressure. From the simulation results, the rate of heat release is directly extracted from the reactive species and their heat formation. By evaluating the heat release rate produced from the engine, the combustion duration can be predicted to maximize the work done when the piston reaches the constant volume stage at the BDC position.

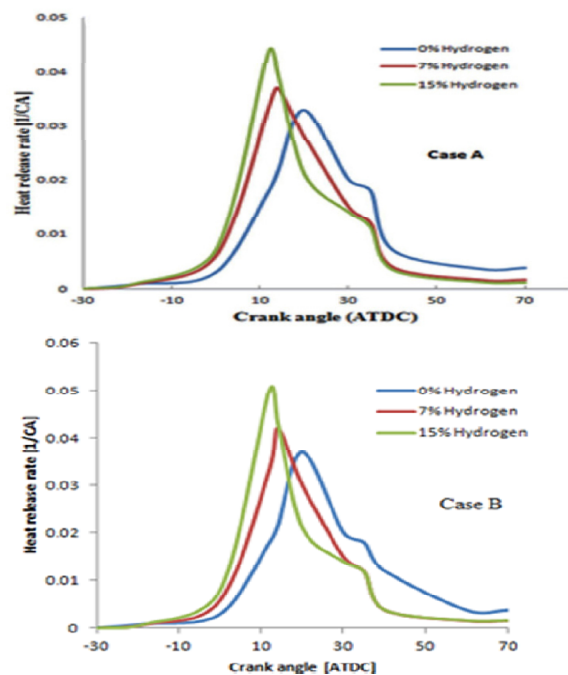


**Figure 8.** Heat release rate versus the CA at a fixed EAR of unit and spark timing of 19°CA BTDC at 2000 (case A) and 6000 rpm (case B)

Based on the theory of combustion, combustion depends on the equivalence ratio, residual fraction, spark timing, laminar flame speed, turbulence intensity of flow, and combustion chamber shape [22].

Figure 8 shows the heat release rate versus of the CA for case A. With the addition of hydrogen to NG, the peak heat release rates increased, and the CAs at which they appeared were advanced.

## 8. Conclusions

In this study, the effects of the addition of hydrogen to NG on a methane-fueled gas engine generator were numerically investigated in terms of engine performance. The results of this study can be summarized as follows:

The percentage of hydrogen in the mixture increases the burning velocity of CNG and decreases with the optimal ignition timing to obtain the maximum peak pressure of the engine running with a blend of hydrogen and CNG. The indicated efficiency rises as the percentage of hydrogen in the mixture increases. Therefore, as the hydrogen fraction is increased, the maximum peak pressure is found to be close to the TDC. With the addition of hydrogen to NG, the peak heat release rates increased, and the CAs at which they appeared were advanced.

For 15% hydrogen, the maximum values for in-cylinder temperature and heat release rate were advanced by approximately  $8^\circ$  CA compared with 0% and 7% hydrogen. The maximum temperature difference between the 0%  $H_2$  and 15%  $H_2$  cases was approximately 150 K.

## 9. References

- [1] K. Zeng, Z. Huang, B. Liu, L. Liu, D. Jiang, Y. Ren, and J. Wang. (2006). Combustion characteristics of a direct-injection natural gas engine under various fuel injection timings, *Applied Thermal Engineering*, 26, 806-813.
- [2] J. Park, H. Cha, S. Song, K. Min Chun. (2011). A numerical study of a methane-fueled gas engine generator with addition of hydrogen using cycle simulation and DOE method, *international journal of hydrogen energy*, 36, 5153- 5162.
- [3] Y. Nakagawa, M. Nakai, K. Hamai. (1982). A study of the relationship between cycle-to-cycle variations of combustion and heat release delay in a spark-ignited engine., *JSME* 25 54–60.
- [4] J.M. Kim, Y.T. Kim, S.Y. Lee, J.T. Lee, (1995). Performance Characteristics of Hydrogen Fueled Engine with the Direct Injection and Spark Ignition System, SAE Paper No. 952498.
- [5] K.S. Varde, G.A. Frame,(2011) Development of a high-pressure hydrogen injection for SI engine and results of engine behavior, *Int. J. Hydrogen Energy*, 10 (11) (1985) 743–748.
- [6] F. Tinaut, A. Melgar, B. Gime'nez, M. Reyes. (2011). Prediction of performance and emissions of an engine fueled with natural gas/hydrogen blends, *international journal of hydrogen energy*, 36,947- 956.
- [7] E. Navarro, J. Leo, R. Corral, (2012). CO2 emissions from a spark ignition engine operating on natural gas–hydrogen blends (HCNG), *Applied Energy*.
- [8] A. Yilanci, I. Dincer& H. Ozturk, (2009).A review on solar-hydrogen/fuel cell hybrid energy systems for stationary applications.*Progress in Energy and Combustion Science*. 35(3), 231-244.
- [9] W. Weindorf& M. Altmann.(2007). LBST Analysis–Yield of biofuels versus hydrogen from photovoltaics and wind power.
- [10] M. Shioji, H. Kawanabe, Y. Taguchi & T. Tsunooka, ( 2004). CFD simulation for the combustion process in hydrogen engines, 15th World Hydrogen Energy Conference (Yokohama, Japan,).
- [11] D. Liu & R. MacFarlane, (1983). Laminar burning velocities of hydrogen-air and hydrogen-air steam flames, *Combustion and Flame*. 49(1), 59-71.
- [12] S. O. Akansu, N. Kahraman, B. Ceper. (2007). Experimental study on a spark ignition engine fueled by methane–hydrogen mixtures, *International Journal of Hydrogen Energy*. 32, 4279–4284.
- [13] J. Wang, Z. Huang, C. Tang, H. Miao, X. Wang, (2009). Numerical study of the effect of hydrogen addition on methane–air mixtures combustion, *International Journal of Hydrogen Energy*. 34, 1084 – 1096.

[14] RL. Hoekstra, K. Collier, N. Mulligan, (1994). Demonstration of hydrogen mixed gas vehicles, 10th World hydrogen Energy Conference. Cocoa Beach, USA, 20–24.

[15] B. Nagalingam, F. Duebel, K. Schmillen, (1983). Performance study using natural gas, hydrogen-supplemented natural gas and hydrogen in AVL research engine. *Int J Hydrogen Energy* 8, 715–20.

[16] A. Mariani, B. Morrone, A. (2012). Unich, Numerical evaluation of internal combustion spark ignition engines performance fueled with hydrogen e Natural gas blends, *International Journal of Hydrogen Energy*. 37, 2644 – 2655

[17] B.E. Poling, J.M Prausnitz, & O.C. John Paul.( 2001). *The properties of gases and liquids*, McGraw-Hill New York.

[18] B.F Magnussen .( 1981). On the structure of turbulence and a generalised eddy dissipation concept for chemical reaction in turbulent flow. *Proceedings of 19th AIAA Aerospace Meeting*.

[19] C. Olikara, and G. Borman.(1975). A computer program for calculation properties of equilibrium combustion products with some applications to IC engines, SAE Paper 1975- 750468.

[20] W.H. Kurniawan, A. Shamsudeen. (2005). CFD investigation and analysis of air motion characteristics for internal combustion engine using 3-d moving mesh model, In: *Proc. of the 8th Int. Conference on Quality in Research (QIR) ME3-CT-04*, (Jakarta, Indonesia).

[21] C.ADAPCO, (2004). *STAR-CD Version 3.22 User Manual and Methodology*. Adapco Group Press.

[22] C.R. Fergusson & A.T. Kirkpatrick. (2001). *Internal combustion engines applied thermo-sciences*, John Wiley and Sons, New York, USA.

